JOURNAL OF VIROLOGY, Sept. 2005, p. 11776–11787 Vol. 79, No. 18
0022-538X/05/$08.00+0 doi:10.1128/JVI.79.18.11776–11787.2005

Green Fluorescent Protein-Tagged Adeno-Associated Virus Particles Allow the Study of Cytosolic and Nuclear Trafficking†

Kerstin Lux,[1] Nico Goerlitz,[1] Stefanie Schlemminger,[2] Luca Perabo,[1,2] Daniela Goldnau,[1,2] Jan Endell,[1,2] Kristin Leike,[1] David M. Kofler,[2] Stefan Finke,[3] Michael Hallek,[1,2,4] and Hildegard Büning[1,2]*

Genzentrum, LMU München, Feodor-Lynen-Str. 25, Munich, Germany[1]; Klinik I für Innere Medizin, Universität zu Köln, Joseph-Stelzmann-Str. 9, Cologne, Germany[2]; Max von Pettenkofer Institut, LMU München, Feodor-Lynen-Str. 25, Munich, Germany[3]; and GSF-National Center for Research and Environment, Marchioninistr. 25, Munich, Germany[4]

Received 1 February 2005/Accepted 14 June 2005

To allow the direct visualization of viral trafficking, we genetically incorporated enhanced green fluorescent protein (GFP) into the adeno-associated virus (AAV) capsid by replacement of wild-type VP2 by GFP-VP2 fusion proteins. High-titer virus progeny was obtained and used to elucidate the process of nuclear entry. In the absence of adenovirus 5 (Ad5), nuclear translocation of AAV capsids was a slow and inefficient process: at 2 h and 4 h postinfection (p.i.), GFP-VP2–AAV particles were found in the perinuclear area and in nuclear invaginations but not within the nucleus. In Ad5-coinfected cells, isolated GFP-VP2-AAV particles were already detectable in the nucleus at 2 h p.i., suggesting that Ad5 enhanced the nuclear translocation of AAV capsids. The number of cells displaying viral capsids within the nucleus increased slightly over time, independently of helper virus levels, but the majority of the AAV capsids remained in the perinuclear area under all conditions analyzed. In contrast, independently of helper virus and with 10 times less virions per cell already observed at 2 h p.i., viral genomes were visible within the nucleus. Under these conditions and even with prolonged incubation times (up to 11 h p.i.), no intact viral capsids were detectable within the nucleus. In summary, the results show that GFP-tagged AAV particles can be used to study the cellular trafficking and nuclear entry of AAV. Moreover, our findings argue against an efficient nuclear entry mechanism of intact AAV capsids and favor the occurrence of viral uncoating before or during nuclear entry.

Adeno-associated virus serotype 2 (AAV2) was discovered as a coinfecting agent during an adenovirus outbreak, without any apparent pathogenicity contributed by AAV (3). Recombinant AAV (rAAV) vectors based on AAV2 or one of the other known serotypes hold an attractive potential for the development of efficient and safe gene therapy vectors. Clinical trials are ongoing for the treatment of cystic fibrosis and hemophilia B (17, 31). Elucidating the molecular mechanisms of viral infection and cellular processing of AAV is critical for the success of these approaches.

Besides conventional biochemical studies, microscopic techniques are emerging as powerful tools for the study of viral infection. A promising development for the investigation of AAV was the finding that viral particles can be labeled by cyanine dyes generating a stable covalent link with amino groups at the capsid surface (2). However, this labeling method is labor intensive and hampered by the low efficiency of the labeling reaction (on average, one dye per capsid) (27). High particle numbers need to be used for fluorescence microscopy studies to overcome this problem. This limitation was conquered by a new technique, single virus tracing (SVT), recently described by our group (27). This method is based on the detection of single molecules with an epifluorescent microscope and a laser beam as a light source, allowing the real-time observation of single virus particles inside living cells. Although it is possible to merge the transmitted-light picture of the cell with the virus-tracking movie by the SVT method, a direct colocalization of virions and cellular organelles remains difficult. Additionally, highly pure viral preparations have to be used to avoid labeling of contaminating proteins. This cannot be achieved easily for many AAV retargeting vectors, since many mutants lose the ability to bind heparan sulfate proteoglycans (HSPGs), preventing the use of heparin affinity chromatography for purification.

Therefore, we aimed to develop an alternative strategy for the labeling of the AAV capsid by using enhanced green fluorescent protein (EGFP). GFP has been extensively used as a fusion protein to study intracellular trafficking and localization of proteins. It has an effective chromophore, which absorbs UV or blue light and emits green fluorescence. No further gene products or substrates are needed. Moreover, GFP does not seem to interfere with cell growth or function. GFP fusion proteins thus provide an attractive tool for biological studies including viral tracking (6, 9, 13, 21, 25, 29, 32, 33).

Different strategies have been previously used to incorporate peptides into the AAV capsid. The capsid is a tightly packaged icosahedron of 25 nm and is composed of three different viral proteins, VP1 (90 kDa), VP2 (72 kDa), and VP3 (60 kDa). These proteins are encoded in the same open reading frame (ORF) and share a common stop codon. They differ

* Corresponding author. Mailing address: University of Cologne, Clinic I for Internal Medicine, LFI, Level 4, Room 052, Joseph-Stelzmann-Str. 9, 50924 Cologne, Germany. Phone: 49-221-478-4448. Fax: 49-221-478-5455. E-mail: buening@lmb.uni-muenchen.de.

† Supplemental material for this article may be found at http://jvi.asm.org/.

in their N termini due to alternative splicing and different initiation codons, resulting in three progressively shorter proteins. Ligand peptides of up to 34 amino acids (aa) have been inserted into aa position 587 of VP1 to generate targeting vectors (11, 24). Peptides were also inserted into the VP1 unique region at aa position 34 (36) and one or two residues downstream from the N-terminal methionine of the VP2 start codon at aa positions 138 (20, 33, 36, 39) and 139 (28). Since VP1 is an N-terminal extension of VP2, insertions at positions 138 and 139 are displayed within VP1 and VP2. The most abundant capsid protein, VP3, remains unmodified. Insertions as large as 32 amino acids were tolerated with only marginally lower packaging efficiencies (20). Larger insertions, for example, the rat fractalkine chemokine domain (76 aa) or the human hormone leptin (146 aa) inserted at aa position 138 resulted in a decrease in VP3 expression, which prevented capsid assembly (33). Providing additional VP3 in *trans* (by a VP3-encoding plasmid) restored capsid assembly with a remaining 5-log decrease in infectivity (33).

However, Yang and colleagues previously showed that large insertions at the N terminus of the VP proteins interfered with capsid assembly (39). In their study, a 29.4-kDa single-chain antibody (designated sFv) was incorporated into the AAV capsid, fusing the sFv gene to the N termini of VP1, VP2, and VP3. The fusion proteins were expressed, but neither the use of all three sFv-VP fusion proteins nor a combination of one sFv-VP with two other unmodified VPs results in detectable rAAV particles. However, when the sFv-VP2 fusion protein was included in the packaging process in the presence of all three unmodified VP proteins, intact rAAV chimeric vector particles containing sFv-VP2 fusion protein were generated. This significantly increased the transduction of target cells expressing a cellular receptor recognized by the inserted antibody.

Based on these previous results, we decided to insert the 27-kDa GFP protein as a GFP-VP2 fusion protein into the AAV capsid. Incorporation of GFP-VP2 into the AAV capsid did not interfere with viral assembly or viral genome packaging. The GFP-tagged virions produced in the present study retained infectivity, in marked contrast to results published by Warrington et al. (33). When used to visualize the process of nuclear entry in more detail, we detected virions in the nuclear area shortly after infection. In agreement with Xiao et al. (37), we observed that adenovirus 5 (Ad5) augmented the efficiency of the nuclear entry of AAV capsids. In cells infected with GFP-VP2–AAV, a colocalization of viral capsids with nuclear invaginations was observed. With prolonged incubation times, the amount of cells displaying AAV capsids within the nucleus increased independently of Ad5 coinfection. However, the majority (>90%) of the capsids remained detectable outside the nucleus during the whole observation period. In contrast, viral genomes were detectable by fluorescence in situ hybridization (FISH) within the nucleus of cells already 2 h postinfection (p.i.), irrespective of Ad5 coinfection, although 10 times fewer virions per cell were used. Compared to 2 p.i. conditions, an increase in the amount of viral genomes was observed at 11 h p.i. Moreover, under these conditions (10^5 instead of 10^6 virions per cell), no intact viral capsids were detected within the nucleus even after prolonged incubation times.

Our studies demonstrate that GFP-VP2-tagged virions are a promising alternative to the chemical labeling of AAV to study the infectious biology of AAV and derived vectors.

MATERIALS AND METHODS

Cell culture. The human cervix epitheloid cell line HeLa (ATCC CCL 2; American Type Culture Collection, Rockville, Md.), the HeLa-DsRed2Nuc cell line (produced by stable transfection of HeLa with pDsRed2-Nuc), and the human embryonic kidney cell line 293 were maintained as a monolayer culture at 37°C and 5% CO_2 in Dulbecco's modified Eagle's medium (DMEM), supplemented with 10% fetal calf serum, 100 U/ml penicillin, 100 mg/ml streptomycin, and 2 mM L-glutamine.

Plasmids. pUC-AV2 (11), pSUB201$^+$ (26), pXX6 (38), and pGFP (15) were described previously. The plasmid pUC-AV2-VP2k.o. was obtained by PCR amplification combined with site-directed mutagenesis of pUC-AV2, changing the ACG start codon into ACC by using overlapping PCR fragments (VP2ko_for, 5′-GTTAAGACCGCTCCGGG-3′; and 4066, 5′-ATGTCCGTCC GTGTGTGG-3′; VP2ko_back, 5′-CCCGGAGCGGTCTTAAC-3′; and 3201, 5′-GGTACGACGACGATTGCC-3′) and ligation of the fragments in a second PCR step with the primers 3201 and 4066. The resulting fragment was digested with BsiWI and EcoNI and sticking-end ligated into pUC-AV2. To obtain the plasmid pGFP-VP2, the sequence encoding VP2 was amplified from pSUB201$^+$ by PCR using the primer pair VP2-N (5′-CTCCGGGAAAAAAGAGG-3′) and VP2-C (5′-TTACAGATTACGAGTCAGGTAT-3′), thereby deleting the VP2 start codon. It was then ligated into pEGFP-C3 (Clontech), which was digested with Bgl II and filled in by Klenow polymerase. The plasmid pDsRed2Nuc was generated by deletion of the EGFP-encoding region from pEGFP-Nuc (Clontech) and insertion of the DsRed2 gene, which was amplified by PCR (the primers used were 5′CGGAGTACATCAATGG-3′ and 5′-AGATCCGGTGG ATCCTACCT-3′) from pDsRed2-N1 (Clontech) and cut with AgeI.

Viral production and purification. AAV particles were produced in HEK293 cells by the adenovirus-free production method with pXX6 (38) to supplement the adenoviral helper functions. Briefly, HEK293 cells were seeded at 80% confluence and cotransfected by calcium phosphate with a total of 37.5 μg of plasmid of pUC-AV2 and pXX6 in a 1:1 molar ratio for the production of wild-type AAV. For the production of chimeric virions, cells were transfected with pXX6, pUC-AV2, and pGFP-VP2, replacing 30% or 60% of pUC-AV2 by pGFP-VP2. For the production of the VP2k.o.-AAV, HEK293 cells were transfected with pUC-AV2-VP2k.o. and pXX6 in a 1:1 molar ratio. For the production of the 100%-GFP-VP2-AAV pUC-AV2-VP2k.o., pGFP-VP2 and pXX6 were transfected at a 1:1:1 molar ratio. At 48 h posttransfection, cells were harvested and pelleted by low-speed centrifugation. Cells were resuspended in 150 mM NaCl–50 mM Tris-HCl (pH 8.5), freeze-thawed several times, and treated with Benzonase for 30 min at 37°C. To purify the viral preparation by iodixanol gradient centrifugation, the cell debris was spun down at 3,700 × *g* for 20 min at 4°C, and the supernatant was loaded onto an iodixanol gradient as previously described (41).

Determination of AAV titers. The particle titers of vector stocks were determined by quantitative PCR (30). Therefore, viral DNA was isolated from vector stocks according to the DNeasy kit protocol (QIAGEN, Hilden, Germany). The capsid titers of vector stocks were determined by A20 enzyme-linked immunosorbent assay (ELISA) as previously described (11). Infectious titers were obtained by infection of HeLa cells as monolayers on coverslips with serial dilutions of viral preparations in the presence of adenovirus type 5 (multiplicity of infection [MOI] of 5). At 72 h postinfection, Rep protein expression was determined by immunofluorescence staining (34). Briefly, cells were fixed in methanol and acetone for 5 min, respectively. After being washed with phosphate-buffered saline (PBS), unspecific reactions were blocked by incubation with 0.2% gelatin in PBS for 10 min. The coverslips were incubated for 1 h at room temperature with the anti-Rep antibody 76/3 (kindly provided by Jürgen Kleinschmidt, DKFZ Heidelberg, Heidelberg, Germany), and coverslips were washed, blocked again, and incubated for 1 h with a secondary antibody (fluorescein isothiocyanate-conjugated goat anti-mouse, 1:100 in PBS; Dianova). Titers were calculated from the last limiting dilution of viral stocks that led to fluorescence-positive cells.

Functional testing of GFP-VP2 fusion protein by transient transfection. HeLa cells (grown on coverslips) were transfected by calcium phosphate precipitation (11) at 80% confluence with the plasmid pGFP-VP2. As a control, HeLa cells were transfected in parallel with pGFP (15). At 48 h posttransfection, cells were fixed for 30 min in 4% paraformaldehyde (PFA). The nuclear lamina was stained as described below by using anti-lamin B antibody.

Western blotting. For the detection of viral capsid proteins, 10^{10} capsids were separated on a sodium dodecyl sulfate-polyacrylamide gel (10% acrylamide) and

blotted onto a nitrocellulose membrane. The membrane was then blocked with 0.2% I-Block (Sigma) in Tris-buffered saline supplemented with Tween 20 overnight at 4°C. After incubation with B1antibody (1:10 in 0.2% I-Block; kindly provided by Jürgen Kleinschmidt, DKFZ Heidelberg, Heidelberg, Germany) and three washing steps in Tris-buffered saline supplemented with Tween 20, the membrane was incubated for 1 h with a peroxidase-conjugated anti-mouse immunoglobulin G (IgG) antibody (1:5,000 in 0.2% I-Block; Sigma). The membrane was washed again, subsequently incubated for 5 min with SuperSignal West Pico Chemiluminescent Substrate (Pierce), and then exposed to Biomax Light Film (Kodak).

Viral infection. A total of 4×10^4 HeLa cells per well were seeded onto 12-mm coverslips inside 24-well plates. After 24 h, HeLa cells were infected with medium with or without 425 units of heparin/ml with 1×10^6 to 5×10^6 capsids/cell. When indicated, cells were coinfected with adenovirus type 5 (MOI of 5). The infection was carried out for 0.5 h on ice. Cells were then shifted to 37°C and incubated at 37°C and 5% CO_2 for the indicated time period. Cells were washed with PBS, fixed for 0.5 h with 3% PFA in PBS at room temperature, and washed again with PBS; the remaining PFA was quenched for 10 min with 50 mM NH_4Cl in PBS. Nuclear staining was obtained by DAPI (4′,6′-diamidino-2-phenylindole; 1 μg/ml in PBS) for 5 min or by anti-lamin B antibody staining. For antibody staining, cells were permeabilized with 0.2% Triton X-100 in PBS for 10 min, blocked for 10 min with 0.2% gelatin in PBS, and then incubated for 1 h at room temperature with the first antibodies, as indicated. As first antibodies, polyclonal goat anti-lamin B IgG antibody (1:50 in PBS; Santa Cruz Biotechnology), monoclonal A20 or B1 hybridoma supernatant derived from mice (kindly provided by Jürgen Kleinschmidt, DKFZ Heidelberg, Heidelberg, Germany) was used. After being washed and blocked, the cells were incubated for 1 h with secondary antibodies. For secondary antibodies, we used Texas Red- or Cy5-conjugated donkey anti-goat antibody (Dianova, diluted 1:50 or 1:100 in PBS; 0.2% gelatin) and Rhodamine Red-X (RRX)-conjugated donkey anti-mouse (Dianova, diluted 1:200 in PBS; 0.2% gelatin). The coverslips were again washed in PBS, embedded in Vectashield mounting medium (Alexis), and examined.

FISH. Plasmid pRC (15), which encodes Rep and Cap of AAV2, was linearized and labeled with 5-(3-aminoallyl)dUTPs by nick translation. Incorporated dUTPs were labeled with amino-reactive Oregon green 488 with the ARES DNA labeling kit (Molecular Probes) according to the manufacturer's manual. To detect the AAV genome inside cells, HeLa cells were prepared as described above. Cells were infected with wild-type AAV2 (10^5 capsids/cell), fixed with 3% PFA after the indicated time points, quenched, and permeabilized as described above. Nuclear lamina and viral capsids were stained by polyclonal goat anti-lamin B IgG antibody and monoclonal A20 hybridoma supernatant derived from mice (kindly provided by Jürgen Kleinschmidt, DKFZ Heidelberg, Heidelberg, Germany). Cy5-conjugated donkey anti-goat antibody (Dianova) and Rhodamine Red-X-conjugated donkey anti-mouse antibody (Dianova) were used as secondary antibodies. After antibody staining, cells were washed with PBS. A hybridization mixture containing 1 ng/μl labeled DNA probe, 50% formamide, 7.3% dextran sulfate, 15 ng/μl salmon sperm DNA, and 0.74× SSC (1× SSC is 0.15 M NaCl plus 0.015 M sodium citrate) was denaturated for 3 min at 95°C and shock cooled on ice. Coverslips were inverted onto the denaturated hybridization mixture (only the DNA probe was denaturated, since the AAV genome is single stranded). Coverslips were sealed with rubber cement, and hybridization occurred at 37°C overnight. The rubber cement was removed, and coverslips were washed three times in 2× SSC at 37°C, three times in 0.1× SSC at 60°C, and two times in PBS. Cells were embedded in Vectashield mounting medium (Alexis).

Wide-field fluorescence microscopy. Images were acquired with an immunofluorescence microscope (Zeiss Axioskop) equipped with filters specific for GFP and DAPI with a 40× (numerical aperture [NA] of 1.3) objective. Images were obtained with a charge-coupled device camera (Visicam; Visitron Systems) with the MetaMorph Imaging System, version 3.0.

Confocal microscopy. To localize the GFP-VP2 signal within the cell more precisely, images were obtained by confocal laser scanning microscopy with a Leica DM IRE2 microscope with a Leica TCS SP2 laser system or a Zeiss Axiovert 200 M microscope with a Zeiss LSM 510 Laser Module, using a 63× (NA 1.4) objective and filter settings optimized for respective dyes. For each sample, a series of 0.2- to 0.25-μm-thick horizontal sections were made. The pinhole was adjusted to 1 airy unit. Images were processed by Leica confocal software or LSM 510 Meta software and Adobe Photoshop, version 7.0.

Live-cell imaging (time lapse microscopy). For live-cell images, 2×10^5 HeLa-DsRed2Nuc cells were seeded onto the glass bottom of microwell dishes (35 mm; Mat Tek). After 24 h, cells were infected with medium with or without 425 units of heparin/ml with approximately 10^6 capsids per cell. Cells were incubated for 20 min at 37°C and then analyzed by live-cell microscopy under physiological conditions. Live-cell movies were obtained with an inverse Zeiss Axiovert 200M microscope with a 63× (NA, 1.4) objective using Zeiss filter sets 10 for GFP and DsRed. Images were taken with a Zeiss Axiocam HRm using the Axiovision 3 software with a time lapse of 30 s.

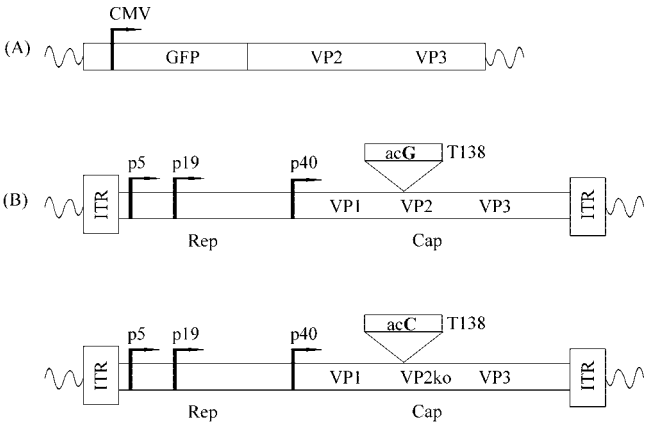

FIG. 1. Schematic representation of the plasmids. (A) The plasmid pGFP-VP2 encodes the GFP-VP2 fusion protein. VP2 was amplified by PCR from pUC-AV2 and cloned into the multiple cloning site of pEGFP-C3 (Clontech). During this step, the VP2 start codon was deleted. (B) To produce wild-type AAV, the plasmid pUC-AV2 was used (top). A G-to-C substitution within the wobble position of the VP2 start codon (T138) was introduced, resulting in the plasmid pUC-AV2-VP2k.o. (bottom). Due to the substitution, VP2 expression was abolished without altering the amino acid sequence of VP1.

Fluorescence-activated cell sorting analyses. A total of 4×10^4 HeLa cells were seeded per well in a 24-well plate. After 24 h, cells were infected with medium with or without 425 units of heparin/ml with 8×10^7 capsids/cell. The virus binding was carried out for 30 min on ice. Thereafter, cells were shifted to 37°C for 1 h. Cells were harvested, resolved in 0.5 ml PBS, and analyzed with a Coulter Epics XL-MCL (Beckman Coulter). A minimum of 5,000 cells was analyzed for each sample. The percentage of positive cells was defined as the fraction beyond the region of 99% of the control of untransfected cells. Data were analyzed with the use of WinMDI 2.8 fluorescence-activated cell sorting software.

RESULTS

GFP fusion does not interfere with nuclear translocation of VP2. EGFP has been widely used as a fusion protein to monitor the cellular localizations of proteins (5). However, it is a relatively large protein to be inserted into a compact structure such as the AAV capsid. Based on the observation that large insertions are tolerated at the N terminus of VP2 (39), we decided to generate a GFP-VP2 fusion protein to incorporate a fluorescent marker into the AAV capsid. For this purpose, the VP2 ORF was amplified by PCR and fused to the C terminus of the GFP ORF (Fig. 1), with the human cytomegalovirus (CMV) promoter controlling transcription. To avoid translation from the natural VP2 start codon, the translation start codon was deleted.

To test the biological properties of this GFP-VP2 fusion protein, transient transfections of HeLa cells with pGFP-VP2 were carried out. As a control, HeLa cells were transfected with a GFP-expressing plasmid lacking any known organelle homing signals (24). At 48 h posttransfection, cells were fixed and the nuclear lamina was stained with an anti-lamin B antibody. Since VP2 contained a nuclear localization sequence (18), GFP-VP2 was expected to be detectable in the nucleus, whereas the GFP lacking homing signals should be distributed

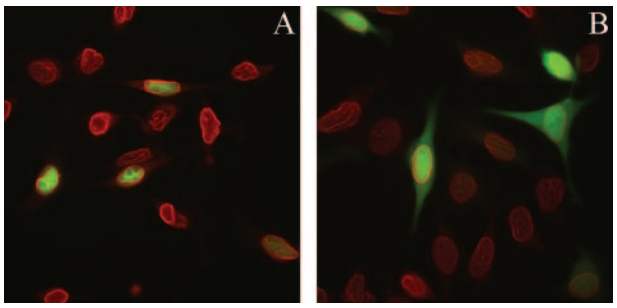

FIG. 2. Transient transfection of HeLa cells with GFP-VP2- and GFP-expressing plasmids. Cells were transfected at 80% confluence with pGFP-VP2 (A) or pGFP (B) and fixed 48 h posttransfection. The nuclear lamina was stained with Texas Red-conjugated anti-lamin B antibody.

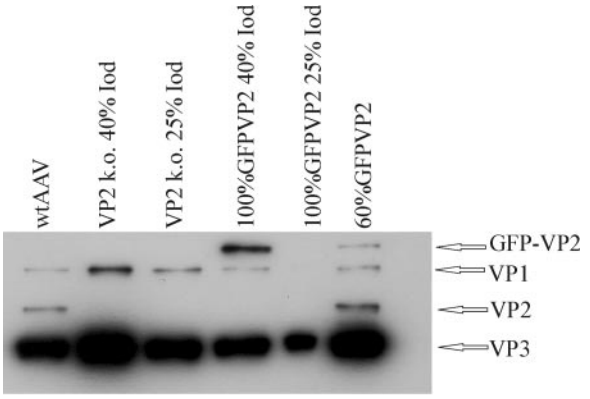

FIG. 3. Western blot analysis of iodixanol gradient-purified AAV capsids. After iodixanol gradient centrifugation, the same amount of viral capsids (10^{10}) of wild-type AAV (lane 1, reading from left to right; 40% phase of iodixanol gradient), VP2k.o.-AAV (lane 2, 40% phase of iodixanol gradient; lane 3, 25% phase of iodixanol gradient), 100%-GFP-VP2-AAV (lane 4, 40% phase of iodixanol gradient; lane 5, 25% phase of iodixanol gradient), and 60%-GFP-VP2-AAV (lane 6, 40% phase of iodixanol gradient) were separated by sodium dodecyl sulfate –10% polyacrylamide gel electrophoresis and analyzed by Western blotting with the B1 antibody.

throughout the whole cell. Figure 2 shows that this was indeed the case, allowing us to conclude that the GFP fusion does not hamper the nuclear localization of VP2.

Replacement of VP2 by GFP-VP2 fusion protein results in infectious virions. In a prior study, scFv-VP2 fusion proteins used to generate viral particles resulted in viral progeny only when all three wild-type AAV capsid proteins were provided during the packaging process (39). Since the size of the GFP insertion was similar to that of scFv, we assumed that all three unmodified wild-type capsid proteins had to be provided during the packaging process to obtain infectious GFP-tagged viral particles. The first step was therefore to determine the amount of VP2 which could be replaced by GFP-VP2 without interfering with the production of infectious AAV particles. We tested 30% and 60% substitutions of pUC-AV2 (encoding the AAV genome) by pGFP-VP2 during packaging. The viral preparations generated were named 30%-GFP-VP2-AAV and 60%-GFP-VP2-AAV, respectively. Wild-type AAV was used as a control. At 48 h posttransfection, virus-producing cells were harvested, and cell lysates were purified by iodixanol step gradients. The 25% and the 40% phases of the gradient were harvested, and genomic and capsid titers were determined. DNA-containing viral particles with comparable titers were detected for the different viral preparations (25% phase of the gradient, 2×10^{10} to 5×10^{10}/ml; 40% phase of the gradient, 0.5×10^{11} to 1×10^{11}/ml). The amount of intact capsids was determined by ELISA with the anti-capsid antibody A20 (35). As expected, a higher amount of empty capsids was obtained in the 25% phase of the gradient. However, all the capsid titers showed comparable values (25% phase of the gradient, $5 \times 10^{13}$to 8×10^{13}/ml; 40% phase of the gradient, 0.4×10^{13} to 1×10^{13}/ml). Thus, neither capsid assembly nor DNA packaging was affected in the 30%- and the 60%-GFP-VP2-AAV preparations in comparison to the wild-type control.

To investigate if the GFP-VP2 fusion proteins were inserted into the AAV capsid and if the GFP-tagged virions retained infectivity, HeLa cells were incubated with the 30%-GFP-VP2-AAV and 60%-GFP-VP2-AAV preparations, respectively. At 2 h p.i., cells were washed intensively, detached from the plate by trypsin treatment, and analyzed by flow cytometry. Treatment with trypsin removes all the proteins bound at the cell surface (1, 22); thus, only intracellular GFP signals should be detected. GFP positive cells were obtained in samples infected with both preparations. The largest amount of GFP-positive cells (19.5%) was obtained with 60%-GFP-VP2-AAV, whereas 13.5% GFP-positive cells were detected by using the same amount of capsids of 30%-GFP-VP2-AAV. In contrast, no green cells were detected when wild-type AAV was used. To exclude pseudotransduction, heparin inhibition controls were included. Heparin, a soluble analogue of the primary AAV receptor HSPG, blocks wild-type AAV infection by binding to the viral capsid. Since the HSPG binding region of AAV is located in the VP3 region of the capsid proteins (36), the ability to bind to these molecules should be retained by the GFP-tagged virions. Incubation of both viral preparations with heparin inhibited cell transduction, indicating that a viral infection and not pseudotransduction was responsible for the GFP signal measured in the GFP-VP2-AAV-infected cells.

These results demonstrate that GFP fusion proteins were incorporated into the AAV capsids of infectious virions and that the GFP signal provided by GFP-tagged virions was detectable by flow cytometry.

Production of GFP-tagged AAV virions in the absence of wild-type VP2. Since comparable titers were obtained for the 30%-GFP-VP2-AAV and 60%-GFP-VP2-AAV preparations, we investigated the possibility of packaging a 100%-GFP-VP2-AAV preparation. A wild-type AAV-encoding plasmid containing a VP2 start codon mutation was generated (pUC-AV-VP2k.o.) (Fig. 1) and used to package 100%-GFP-VP2-AAV. In addition, VP1/VP3-only particles (VP2k.o.AAV), 60%-GFP-VP2-AAV, and wild-type AAV were produced and purified by density gradient centrifugation. First, a Western blot analysis of our different preparations was performed (Fig. 3). Although only virions isolated from the 40% phase of the iodixanol gradient were used for the following studies, the 25% phase of the gradient was also analyzed by Western blotting. For wild-type AAV, we obtained three signals corresponding to VP1, VP2, and VP3 (Fig. 3, lane 1) at a ratio of approxi-

TABLE 1. Characterization of the different viral preparations

Preparation[d]	Genomic particles/ml	Physical particles/ml	Infectious particles/ml	Empty/full ratio	Genomic particle/infectivity ratio
Wild-type AAV[a]	2.49×10^{11}	1.25×10^{13}	8.38×10^{9}	50.2	29
Wild-type AAV[b]	1.04×10^{12}	1.19×10^{13}	1.67×10^{10}	11.4	62
VP2 k.o.-AAV[a]	1.30×10^{11}	9.39×10^{12}	1.31×10^{8}	72.2	991
VP2 k.o.-AAV[b]	1.17×10^{12}	1.41×10^{13}	4.19×10^{9}	12.1	278
60% GFP-VP2-AAV[a]	7.01×10^{11}	1.04×10^{13}	8.38×10^{9}	14.8	84
60% GFP-VP2-AAV[b]	2.15×10^{11}	1.25×10^{13}	2.10×10^{9}	58.1	102
60% GFP-VP2-AAV[c]	4.10×10^{11}	7.35×10^{12}	2.10×10^{9}	17.9	195
100% GFP-VP2-AAV[a]	3.00×10^{11}	1.36×10^{13}	1.31×10^{8}	45.3	2,288
100% GFP-VP2-AAV[b]	4.39×10^{11}	9.71×10^{12}	2.10×10^{9}	22.2	208
100% GFP-VP2-AAV[c]	1.5×10^{12}	1.09×10^{13}	1.05×10^{9}	7.2	1,431

[d] Titers were determined by quantitative PCR, Azo ELISA, and infectious titer assay, respectively (*a*, *b*, and *c* indicate viral preparations that were independently packaged.

mately 1:1:20. As expected, VP2k.o.-AAV contained only VP1 and VP3 proteins (lanes 2 and 3), whereas in the 100%-GFP-VP2-AAV preparation the GFP-VP2 fusion protein, VP1, and VP3 were detected (lane 4). The 60%-GFP-VP2-AAV was packaged in the presence of all three unmodified AAV capsid proteins; four protein bands (GFP-VP2, VP1, VP2, and VP3) were visible (lane 6).

Further, we performed a detailed titer analysis. Therefore, each virus mutant was packaged at least a second time. The capsid, genomic, and infectious titers of these preparations were determined, and empty-to-full and genomic particle-to-infectivity ratios were calculated to directly compare the different preparations for packaging efficiency and infectivity (Table 1). No significant difference between mutants (including the wild type) was observed for genomic or capsid titers, which ranged between 1.3×10^{11} and 1.5×10^{12} per ml and 7.35×10^{12} and 1.36×10^{13} per ml, respectively. The ratios of empty-to-full capsids varied to nearly the same extent for different preparations of the same virus mutant (including the wild type) as between the different mutants. This reveals that the deletion of VP2 or the replacement by GFP-VP2 does not interfere with capsid formation or viral genome packaging. The genomic particle-to-infectivity ratios were slightly increased for VP2k.o.- and the 100%-GFP-VP2-AAV-preparations but remained within the variation described for wild-type AAV preparations (11, 14, 24).

The results revealed that GFP-tagged virions with a 100% replacement of VP2 by GFP-VP2 can be generated with high titers (2×10^{9} infectious particles/ml).

Visualization of viral infection by GFP-VP2-tagged AAV particles. To determine if GFP-tagged virions were suited for intracellular visualization, viral infections of HeLa cells followed by wide-field fluorescent microscopic analysis 2 p.i. were performed. GFP signals seemed to localize partly in the nucleus or perinuclear area in cells infected with the 60%- and 100%-GFP-VP2-AAV preparations (Fig. 4A and B). The fluorescent microscopy images obtained thus resembled published results with unlabeled or chemically labeled virions (2, 37). No signal was detected inside the cell when soluble heparin was used, demonstrating that the GFP signal was not due to pseudotransduction (Fig. 4C).

A promising development in the field of fluorescent microscopy is live-cell imaging. Infection of live HeLa cells with GFP-tagged AAV virions, followed by live-cell imaging micros-

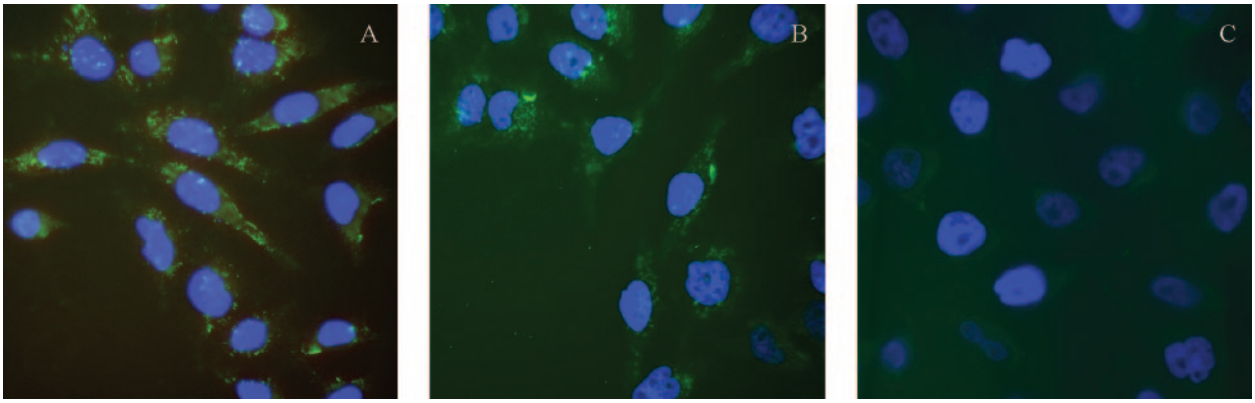

FIG. 4. GFP-tagged virions analyzed by wide-field fluorescent microscopy. Cells were infected with 5×10^{6} capsids per cell of 100%-GFP-VP2-AAV (A) and 60%-GFP-VP2-AAV (B and C) in the absence (A and B) or presence (C) of heparin. Cells were fixed, and nuclei were stained with DAPI.

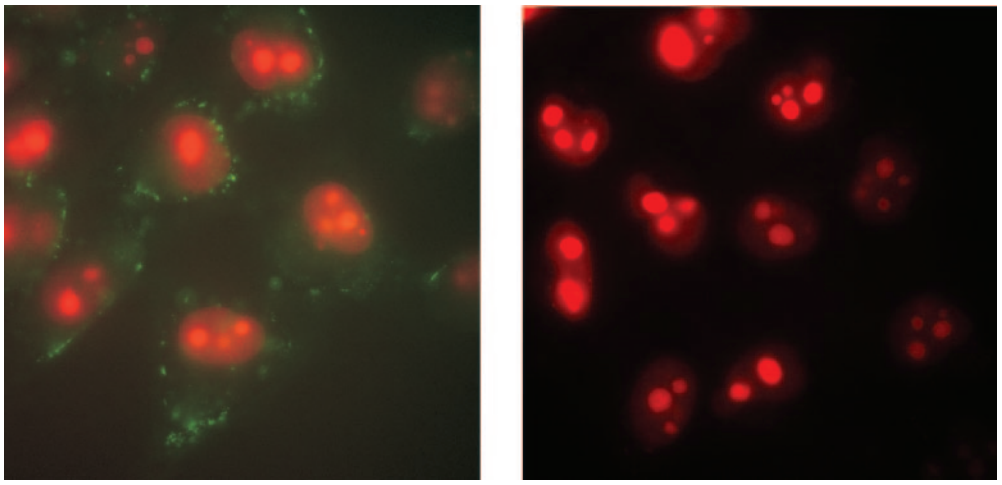

FIG. 5. Live cell imaging of GFP-tagged virions. HeLa-DsRed2Nuc cells were infected with 60%-GFP-VP2-AAV (10^6 capsids per cell). Cells were incubated for 20 min at 37°C and 5% CO_2. Then, live-cell movies were obtained under physiological conditions. (Left) The still image shown here was obtained from the movie supplied in the supplemental material; (right) heparin control.

copy, allowed the visualization of virions undergoing cell membrane contact (Fig. 5; see the movie in the supplemental material). Some of these virions touched the cell membrane multiple times similar to the observations, made previously by SVT (27). As observed by fluorescent microscopy, most of the virions stacked to the membrane, again confirming previous SVT observations, which showed that less than half of the virions entered the cell (27). Furthermore, GFP-tagged virions seemed to move inside the cytoplasm of infected cells and in the perinuclear area (Fig. 5; see the movie in the supplemental material), suggesting the potential of this technology for real-time imaging studies.

GFP-tagged virions within the cell are recognized by A20. To assess if the GFP signals within the cell are emitted from intact viral particles, cells were infected with 100%-GFP-AAV and fixed at 2, 4, 11, and 24 h p.i. Intact viral capsids were stained by A20 (A20 recognizes whole but not dissociated AAV capsids) (4), whereas an anti-lamin B antibody was used to visualize the nuclear membrane. Figure 6 shows one example obtained by confocal microscopy. GFP-tagged AAV particles recognized by A20 were detected within the cell and above the nuclear membrane. An almost 100% colocalization of the GFP signals (Fig. 6, upper left) with A20-reactive AAV capsids (upper right) was observed (merged data are shown in Fig. 6, lower right). The few detectable noncolocalized signals were due to a very faint A20 signal, which became visible after enhancing its excitation energy. Thus, GFP signals visible within the cells emanate from intact virions.

Viral capsids do not enter the nucleus efficiently. To analyze the time course of nuclear entry of AAV in more detail, HeLa cells were infected with 100%-GFP-VP2-AAV for 2, 4, 11, and 24 h with or without adenovirus type 5 coinfection (MOI of 5); confocal laser scanning images were obtained. For each image, a series of horizontal sections, was prepared by taking images (each 0.2 um; z-stack) and superimposed with the Leica confocal software. Figure 7B shows a typical image obtained 4 p.i. without adenovirus coinfection. Many GFP signals were visible in the nuclei of the infected cells (nuclear lamina were stained red by anti-lamin B antibody). This image led to the assumption that GFP-tagged virions were efficiently transported into the nucleus in <4 h, consistent with previously published results (2). However, the Leica confocal software enabled the vertical sectioning of the superimposed pictures and allows visualization of a certain image plane within this stack. The investigator can determine if a certain signal emanates within, above, or below the image plane; this enables the investigator to localize the object of interest more precisely. Using this

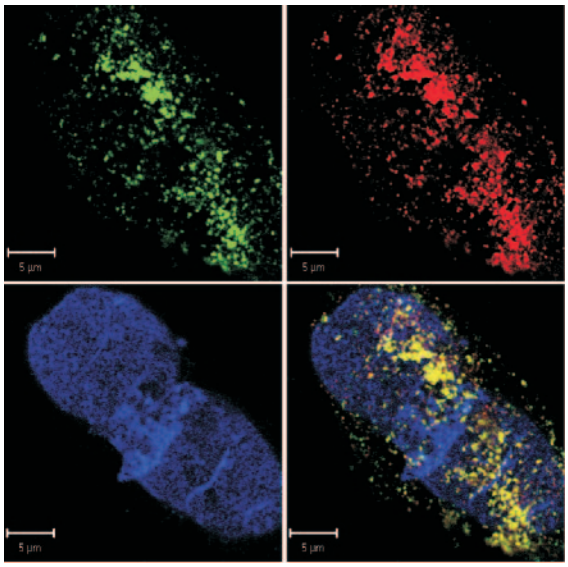

FIG. 6. Intact 100%-GFP-VP2-AAV particles within the cell. HeLa cells were infected with 100%-GFP-VP2-AAV (10^6 capsids per cell). At 4 h p.i., cells were fixed and stained with A20 (recognizes intact AAV capsids; RRX-conjugated secondary antibody), and anti-lamin B antibody (nuclear membrane; Cy5-conjugated secondary antibody). Upper left panel, GFP staining; upper right panel, A20 staining; lower left panel, anti-lamin B; lower right panel, merge. Analysis was performed by confocal microscopy.

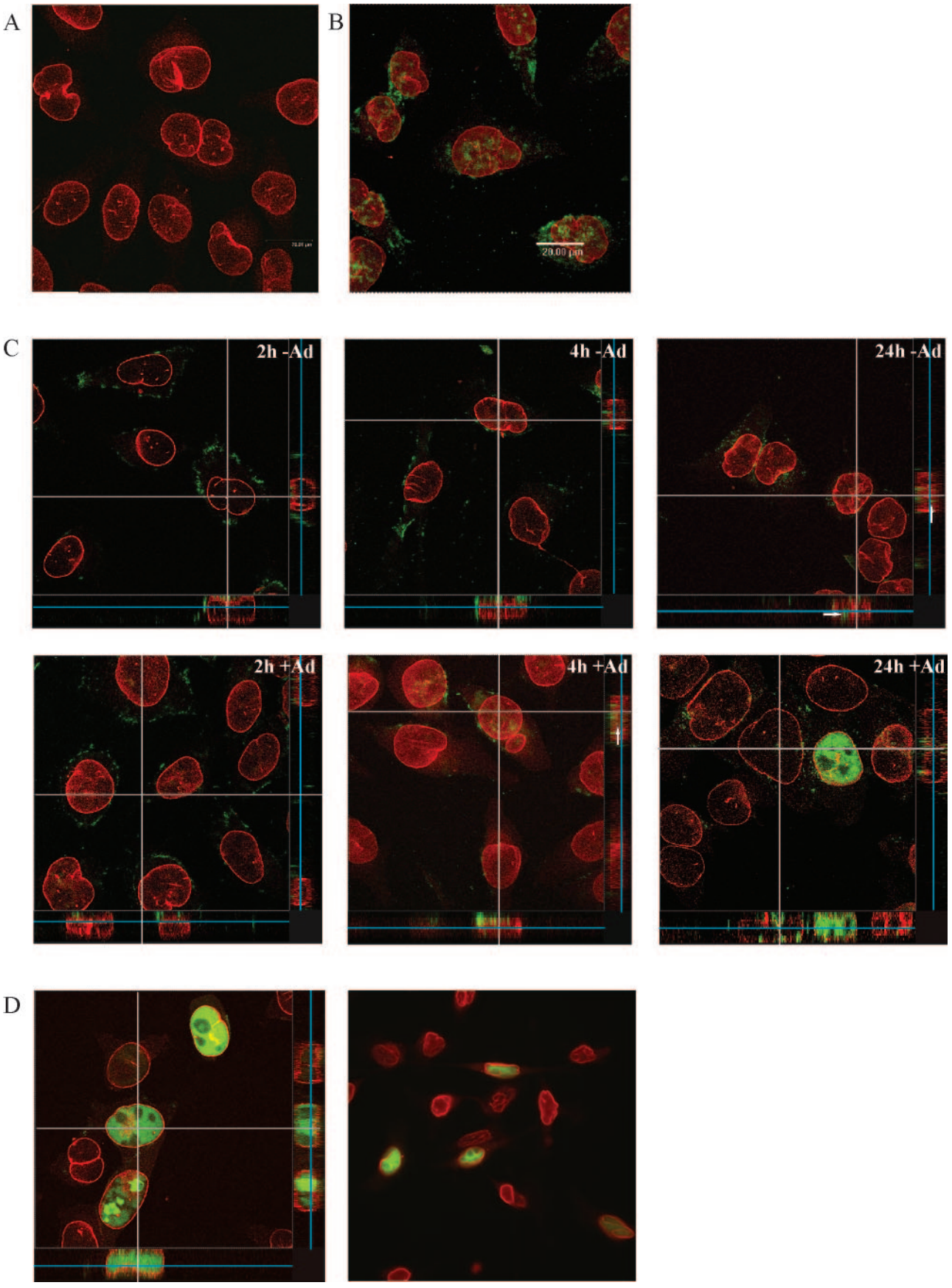
A
B
20.00 µm
C
2h -Ad
4h -Ad
24h -Ad
2h +Ad
4h +Ad
24h +Ad
D

technique, we could determine that in the absence of helper virus and up to 4 h p.i., the GFP signals (from the GFP-tagged virions) were localized above but not within the nucleus (Fig. 7C, top rows). This is in contrast to results derived from the superimposed picture (Fig. 7B) indicating its limitations. At 24 h p.i., isolated signals were visible inside the nucleus (Fig. 7C, arrows in top rows).

Moreover, in the superimposed picture of cells coinfected with adenovirus, many GFP signals were observed in the nucleus 2 h p.i. Applying the new vertical sectioning method uncovered that most of the signals are localized above the nucleus (Fig. 7C, bottom rows). With prolonged incubation time, the amount of coinfected cells showing a GFP signal inside the nucleus slightly increased (e.g., 4 h p.i.), but the majority of signals were still found outside the nucleus. Even after prolonged incubation (up to 11 h; data not shown) >90% of the GFP signals remained outside the nucleus.

Interestingly, at 24 h p.i., many coinfected cells showed a diffuse GFP distribution within the nucleus. This phenomenon was not observed in the absence of helper virus coinfection, even after prolonged observation times (48 h) (data not shown). Since this image resembled the image obtained after transfection with pGFP-VP2 (Fig. 7D), we analyzed the viral preparations used to infect the cells and the respective virus-infected cells by PCR. These analyses revealed that GFP sequences were packaged into the viral capsid, although the plasmid used to express GFP-VP2 during the packaging process contained no AAV inverted terminal repeats. It remains to be elucidated whether this is attributed to recombination or to other events.

To exclude that the observed results are due to inefficient nuclear transport of the GFP-tagged virions, the same experiments were performed with wild-type AAV in Ad5-coinfected cells. For detection of viral capsids and viral capsid proteins, A20 and B1 antibodies were used, respectively. A20 recognizes intact but not dissociated AAV capsids, whereas B1 binds to amino acids 726 to 733 at the C termini of all three capsid proteins (4). At 2, 4, and 11 h p.i., almost no B1 staining was detectable, in marked contrast to A20 staining (data not shown). At 4 and 11 h p.i., no difference was observed when GFP-tagged virions were compared to wild-type virions (for an example at 11 h p.i., see Fig. 9B). At these time points, only isolated intact capsids (recognized by A20) were found within the nucleus; the majority (over 90%) of the virions were visible outside the nucleus (see Fig. 9B). At 24 h p.i., both antibodies were able to recognize their targets and resulted mainly in a nuclear staining (data not shown). This suggests that at this time point, new viral capsid proteins were synthesized in the Ad5-coinfected cells, and new capsids were formed.

From these data, we propose that an adenoviral function augments the nuclear translocation of viral capsids. However, the low level of GFP or A20 signals detected within the nucleus suggests a very inefficient nuclear translocation. Thus, uncoating seems to occur before or during nuclear entry.

To further investigate this hypothesis, HeLa cells were infected by wild-type AAV using 10 times fewer virions per cell. Infections were performed with and without helper virus. Since viral replication in adenovirus-coinfected cells is reported to start between 8 and 12 h p.i (23, 37), infections were stopped at 2, 4, and 11 h p.i. To visualize viral genomes, FISH was performed. In addition, viral capsids and the nuclear lamina were stained by antibodies (Fig. 8A and B). Viral genomes were detectable outside and within the nucleus at 11 p.i. (Fig. 8A and arrows in Fig. 8B). No colocalization of viral genomes and intact viral capsids was observed within the nucleus, whereas colocalizations were detectable in the perinuclear area and within the cytoplasm (red signals in Fig. 8A and in the merged image indicate intact capsids recognized by AZO). In addition, empty capsids (no colocalization) were visible in the perinuclear area. Some of the FISH signals in the perinuclear area showed no colocalization with A20 and therefore with intact capsids. It has yet to be investigated if these signals emanated from free viral genomes or if they colocalized with one of the three VP proteins. The same image was obtained by using a comparable amount of viral genomes in the absence of helper virus, revealing that the observed viral genomes originate from incoming virions and are not the result of viral replication. Furthermore, it allows the assumption that a nearly comparable nuclear transport of viral genomes occurs with or without helper virus. Interestingly, viral genomes within the nucleus were already detectable at earlier time points (2 and 4 h p.i.) both in the presence and absence of Ad5, although 10 times fewer virions per cell were used than for the capsid studies (Fig. 6, 7, and 9). Under these conditions (10^5 instead of 10^6 capsids per cell), viral capsids are detected within the cell, but none of these localized within the nucleus (Fig. 8B).

All these observations strongly support the hypothesis that uncoating of AAV occurs during or before nuclear entry. However, at the present time, it cannot be excluded that viral genomes within the nucleus are associated with one of the three viral capsid proteins.

AAV is found in nuclear invaginations. Single particles have been shown to reach the nuclear area within seconds (27), and a perinuclear accumulation of AAV was found to occur within 1 to 2 h p.i (2, 37). Interestingly, we observed in addition AAV particles within tubular channels, which extended deeply into the nucleoplasm (Fig. 9). This could first be assumed from SVT analysis. With our SVT studies, we had observed that AAV moved very quickly on certain "pathways" through the

FIG. 7. Time course of AAV infection visualized by GFP-tagged AAV virions. HeLa cells were infected with 10^6 capsids per cell of 100%-GFP-VP2-AAV with or without adenovirus type 5 (MOI of 5) coinfection. In addition, a heparin control was included (A). At 2, 4, and 24 h p.i., cells were fixed and the nuclear lamina was stained with Texas Red-conjugated anti-lamin B antibody. A series of horizontal sections (each 0.2 μm) were obtained for each panel. With Leica confocal software, all images of a series were superimposed. (B) Superimposed image of a series of sections 4 h p.i. in the absence of adenoviral coinfection. (C) Time course of infection with and without adenovirus (Ad5) coinfection. The square image of each panel shows one horizontal section of the stack. The vertical sections of the stack are depicted on the right and bottom of each panel. Arrows show GFP signals detected within the nucleus. (D) Comparison of images obtained 24 h p.i. in the presence of adenovirus (left) and after transfection of pGFP-VP2 (right).

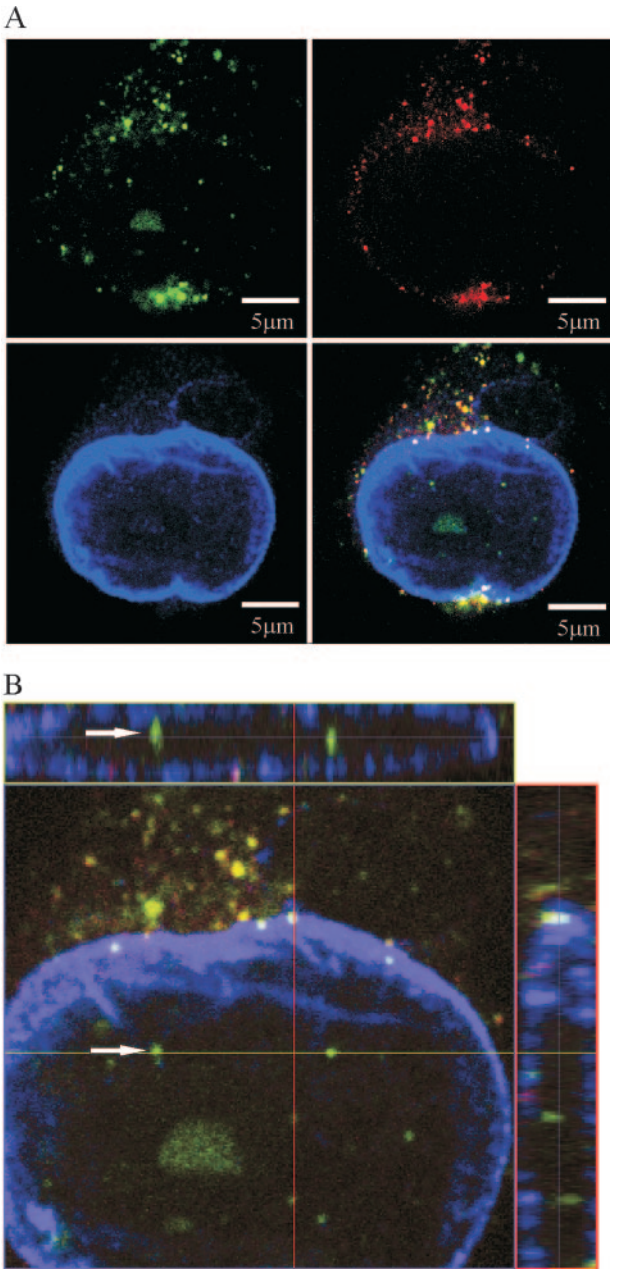

FIG. 8. Visualization of viral genomes by FISH. (A) HeLa cells were infected with wild-type AAV (10^5 capsids per cell = 8,700 genomic particles per cell) and adenovirus type 5 (MOI of 5). Cells were fixed 11 h p.i. and FISH (green, Oregon green-labeled DNA probe) was performed to visualize viral genomes, whereas intact capsids and nuclear membrane were stained using A20 (red, RRX-conjugated secondary antibody) and anti-lamin B antibody (blue, Cy5-conjugated secondary antibody), respectively. Analyses were performed by confocal microscopy and one image plane out of a z-stack is shown (top left, FISH; top right, A20; bottom left, anti-lamin B; bottom right, merge). (B) Enlargement and vertical sectioning of merge shown in panel A. The arrows show one example of a viral genome localized within the nucleus. The green signal indicates the viral genome visualized by FISH, using Oregon green-labeled DNA probe; red signal indicates intact capsids visualized by A20 and an RRX-conjugated secondary antibody; blue signal indicates nuclear lamina visualized by anti-lamin B and Cy5-conjugated secondary antibody. Cy5-conjugated secondary antibody.

nuclear area; we hypothesized that these pathways were nuclear invaginations, which are tubular structures derived from the nuclear envelope. The enclosed core is continuous with the cytoplasm and may function to bring larger proportions of the nucleoplasm close to a nuclear pore (10). In addition, a function of these nuclear channels in transport processes has been previously proposed (8). Within our present analysis, we observed AAV particles within nuclear invaginations (visualized by nuclear laminar staining), which verify our former assumptions (27). These pictures were obtained for both, the GFP-tagged virions (Fig. 9A and C) and wild-type AAV (Fig. 9B). The capsids were recognized in both cases by A20 revealing that intact viral capsids were detected within the nuclear invaginations. Although the significance of this colocalization has to be clarified, it explains the directed motion along defined pathways through the nuclear area observed by SVT.

DISCUSSION

To track the intracellular trafficking of AAV and derived vectors in infected cells, we tagged virions by incorporation of GFP-VP2 into the viral capsid. In a first step, chimeric virions containing VP1, VP2, GFP-VP2, and VP3 were produced. GFP-tagged AAV particles could also be generated without the addition of wild-type VP2. This observation is in contrast to that of Yang et al. (39), who showed that the AAV capsid is not able to tolerate large insertions at the N terminus of VP2 without the simultaneous addition of wild-type VP2. This discrepancy might be due to differences in the production and purification method: Yang et al. expressed the different VP proteins from three different plasmids controlled by the CMV promoter and used a CsCl density gradient for purification. In addition, remaining helper virus was inactivated by heat. Use of natural AAV viral promoters and a helper virus-free production method allowed efficient generation of particles with N-terminal VP2 fusions of different sizes (20, 28, 33, 36). The largest insertion described so far is the 30-kDa GFP protein used by Warrington et al. and by us. Interestingly, although Warrington and colleagues used the same amino acid position (aa 138) for the VP2 fusion, the genomic particle-to-infectivity ratio reported by Warrington et al. was remarkably higher (up to 130-fold less infectious) than ratios obtained for our GFP-tagged virions (33). In addition, an up to 30-fold-larger amount of empty capsids was detected within the study by Warrington et al. We observed a genomic particle-to-infectivity ratio between 84 and 195 for 60%-GFP-VP2-AAV and between 208 and 2288 for the 100%-GFP-VP2-AAV, which is higher than ratios obtained for the wild-type AAV within our study (i.e., 29 and 62), but still in the range previously described for wild-type preparations (24). Furthermore, no increase in the amount of empty capsids was detected. Since we used the same amino acid position for the fusion (aa 138), the differences observed must have been caused by other factors. One main difference could be the choice of the promoter responsible for the transcription of VP2. Warrington et al. used the natural p40 promoter, and translation was initiated from a modified and therefore stronger start codon (ATG instead of ACG), which resulted in a more efficient VP2 and in the inhibition of VP3 initiation from this template. In our case, the viral CMV pro-

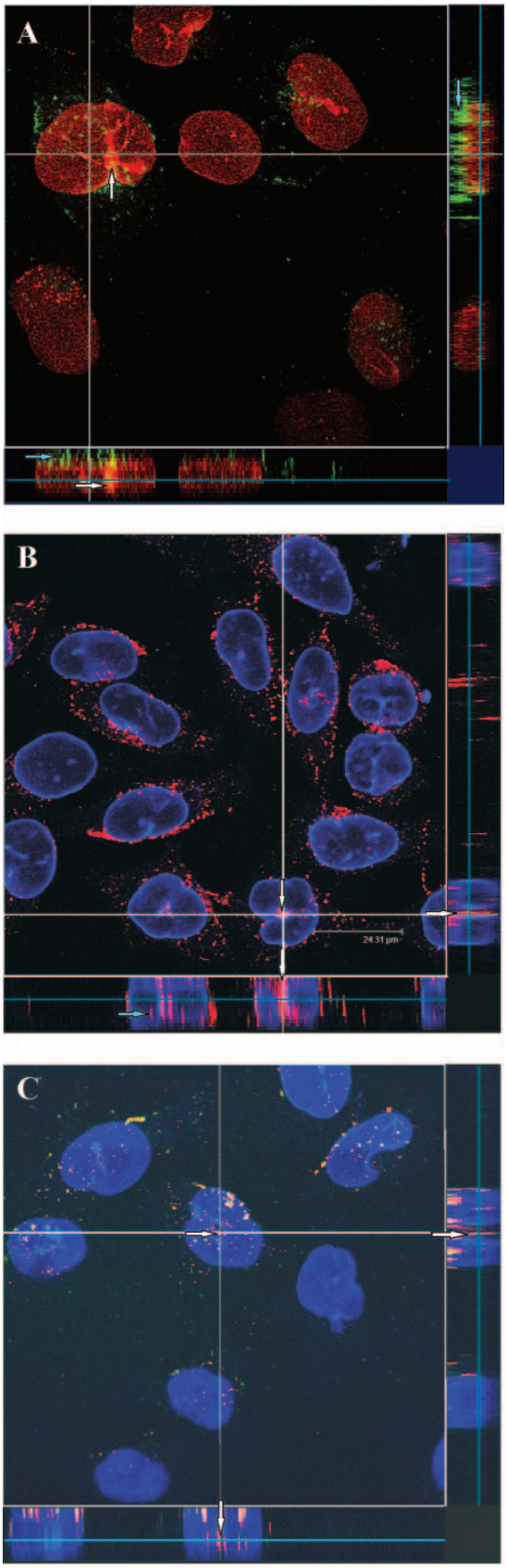

moter was used to control the transcription of the fusion protein and the VP2 translation start codon was deleted. Warrington and colleagues performed a Western blot of their GFP-tagged virions. When comparing their Western blot results with the results obtained for our GFP-tagged virions packaged in the presence of pGFP-VP2 (Fig. 3), the most obvious difference was the amount of VP1 detected in the GFP-tagged virion preparations. While the preparations of Warrington and colleagues showed a clear reduction for the VP1 signal, the amount of VP1 in our preparations was comparable to that of wild-type AAV. It is known that VP1—possibly because of its phospholipase activity—is essential for AAV infectivity (4, 12, 19, 40). Therefore, the reduced amount of VP1 in the preparations used by Warrington et al. might be a reasonable explanation for the lower infectivity of the vectors they produced and the discrepancy with our results. It remains unknown if the modification of the VP2 translation start codon as carried out by Warrington and colleagues is responsible for the VP1 reduction, or if other factors are at work. However, our preparations yielded an up to 130-fold increased viral infectivity in comparison to the results of Warrington et al., with an infectious titer of 10^9 per ml. The GFP-tagged virions produced in our study were comparable to wild-type AAV. This assumption is based on our direct comparison with wild-type AAV and on antibody colocalization studies (Fig. 6 and 9).

According to the current model of AAV infection, AAV enters host cells by receptor-mediated endocytosis, which is a very fast process that occurs in approximately 60 ms (27). Within the first 10 min, two-thirds of membrane bound virus particles is internalized (2). The endocytotic process and the subsequent trafficking steps are still poorly understood and may differ substantially in different cell types, and in some cases even in the same cell types (7, 16). The release of AAV from the endosomes is believed to take place at the late endosomal stage and requires a low endosomal pH (2). There-

FIG. 9. AAV with nuclear invaginations. (A) HeLa cells were infected with 10^6 capsids per cell of 100%-GFP-VP2-AAV. At 11 h p.i., cells were fixed, and the nuclear lamina was stained with Texas Red-conjugated anti-lamin B antibody. Analysis was performed by confocal microscopy. A series of horizontal sections (each 0.2 μm) were obtained for each image. The square image shows one horizontal section of the stack. The vertical sections of the stack are depicted on the right and bottom of each panel. White arrows, capsid in nuclear invaginations; blue arrows, capsid in perinuclear area. (B) HeLa cells were infected with 10^6 capsids per cell of wild-type AAV and adenovirus type 5 (MOI of 5). At 11 h p.i., cells were fixed. Capsid and nuclear membrane were stained with A20 (red; RRX-conjugated secondary antibody) and anti-lamin B antibody (blue; Cy5-conjugated secondary antibody), respectively. Microscopic analyses were performed as described in the legend to panel A. Under these conditions, isolated signals of intact capsid were detectable inside the nucleus (blue arrow). In addition, viral capsids within nuclear invaginations were observed (white arrow). (C) HeLa cells were infected with 10^6 capsids per cell of 100%-GFP-VP2-AAV and coinfected with adenovirus type 5 (MOI of 5). At 2 h p.i., the cells were fixed. Capsids and nuclear membrane were stained with A20 (red; RRX-conjugated secondary antibody) and anti-lamin B antibody (blue, Cy5-conjugated secondary antibody), respectively. Microscopic analyses were performed as described in the legend to panel A. GFP-tagged virions in nuclear invaginations were recognized by A20 (white arrow).

after, the destiny of AAV remains unclear. Some studies have observed perinuclear accumulation within 1 to 2 h p.i., which persisted in the absence of adenovirus coinfection for at least 16 h (33, 37). In contrast, by laser scanning confocal microscopy, Bartlett et al. observed AAV particles within the nucleus of infected cells by 2 h p.i., despite the absence of helper virus (2).

In this study, we observed that intracellular trafficking of GFP-tagged virions occurred quickly, at least in HeLa cells. This was in agreement with results obtained with SVT. This sensitive method allows the observation of single particles in a living cell. Due to this high level of sensitivity, it was possible for us to detect at least one AAV particle in the nuclear area of 50% of the cells by 15 min p.i. In some cases, AAV reached the nuclear area within seconds (27). In contrast to this, the nuclear entry of intact AAV capsids is comparably slow. Although many virions already accumulated in the perinuclear area before 2 h p.i., with the absence of helper virus coinfection we observed only isolated GFP signals from the GFP-VP2-AAV particles within the nucleus of cells at 11 and 24 h p.i. (no signal at 2 or 4 h p.i.). This result clearly contradicts results described by Bartlett et al., who observed the absence of helper virus AAV particles inside the nucleus by 2 h p.i (2). This can be explained by the limited microscopic possibilities available at that time.

In adenovirus-coinfected cells, GFP signals were observed within the nucleus by already 2 h p.i. (the earliest time point observed), revealing that adenovirus is able to augment nuclear entry of AAV capsids. These results confirm previous observations that described intact viral particles within the nucleus of coinfected cells in <1 h p.i (33, 37). However, the amount of AAV capsids we observed by applying the new vertical sectioning method for data analysis was much lower than described by (for example) Xiao et al. (37). In all conditions and at all time points analyzed during this study, only very few GFP signals provided by the GFP-VP2-AAV particles could be detected within the nucleus. This was not due to the GFP-VP2-AAV virions used to analyze this step of the infectious biology, since the same image was obtained with wild-type AAV visualized by A20 (Fig. 9).

We assume that the transport of intact viral capsids into the nucleus of infected cells is a very inefficient process and that viral uncoating takes place before or during nuclear entry, independently of helper virus coinfection. The very small amount of intact particles observed in the nucleus of cells infected with 10^6 viral capsids per cell could be due to unspecific events and is likely to be unnecessary for viral replication. This model is suggested by the comparison of the amount of viral genomes with the amount of capsids detected within the nucleus at different time points of the infection in the presence and absence of helper virus: neither in the presence nor in the absence of helper virus intact were viral capsids detected within the nuclei of cells infected with 10^5 (instead of 10^6) viral capsids per cell. In contrast, under the same conditions viral genomes were detected by 2 h p.i. within the nucleus, with a slight increase in signals with prolonged observation times. This argues for an uncoating of AAV before or during nuclear entry independent of helper virus coinfection.

ACKNOWLEDGMENTS

This work was supported by the Deutsche Forschungsgemeinschaft (SFB 455 [M.H., L.P., J.E., D.G., S.F., and H.B.] and SP 658/2-1 [K.L., M.H., and H.B.]), the Promotionsstudiengang Molekulare Medizin (N.G.), and the Bayerische Forschungsstiftung (M.H. and H.B.).

Furthermore, we thank Richard Jude Samulski (University of North Carolina at Chapel Hill) for kindly providing pXX6 and Jürgen Kleinschmidt (DKFZ Heidelberg, Heidelberg, Germany) for kindly providing us with the A20 and B1 antibodies.

REFERENCES

1. **Awedikian, R., A. Francois, M. Guilbaud, P. Moullier, and A. Salvetti.** 2005. Intracellular route and biological activity of exogenously delivered Rep proteins from the adeno-associated virus type 2. Virology **335:**252–263.
2. **Bartlett, J. S., R. Wilcher, and R. J. Samulski.** 2000. Infectious entry pathway of adeno-associated virus and adeno-associated virus vectors. J. Virol. **74:** 2777–2785.
3. **Blacklow, N. R.** 1988. Adeno-associated virus in humans, p. 165–174. *In* J. R. Pattison (ed.), Parvoviruses and human disease. CRC Press, Inc., Boca Raton, Fla.
4. **Bleker, S., F. Sonntag, and J. A. Kleinschmidt.** 2005. Mutational analysis of narrow pores at the fivefold symmetry axes of adeno-associated virus type 2 capsids reveals a dual role in genome packaging and activation of phospholipase A2 activity. J. Virol. **79:**2528–2540.
5. **Chalfie, M., Y. Tu, G. Euskirchen, W. W. Ward, and D. C. Prasher.** 1994. Green fluorescent protein as a marker for gene expression. Science **263:**802–805.
6. **Desai, P., and S. Person.** 1998. Incorporation of the green fluorescent protein into the herpes simplex virus type 1 capsid. J. Virol. **72:**7563–7568.
7. **Duan, D., Y. Yue, Z. Yan, J. Yang, and J. F. Engelhardt.** 2000. Endosomal processing limits gene transfer to polarized airway epithelia by adeno-associated virus. J. Clin. Investig. **105:**1573–1587.
8. **Dupuy-Coin, A. M., P. Moens, and M. Bouteille.** 1986. Three-dimensional analysis of given cell structures: nucleolus, nucleoskeleton and nuclear inclusions. Methods Achiev. Exp. Pathol. **12:**1–25.
9. **Elliott, G., and P. O'Hare.** 1999. Live-cell analysis of a green fluorescent protein-tagged herpes simplex virus infection. J. Virol. **73:**4110–4119.
10. **Fricker, M., M. Hollinshead, N. White, and D. Vaux.** 1997. Interphase nuclei of many mammalian cell types contain deep, dynamic, tubular membrane-bound invaginations of the nuclear envelope. J. Cell Biol. **136:**531–544.
11. **Girod, A., M. Ried, C. Wobus, H. Lahm, K. Leike, J. Kleinschmidt, G. Deleage, and M. Hallek.** 1999. Genetic capsid modifications allow efficient re-targeting of adeno-associated virus type 2. Nat. Med. **5:**1052–1056.
12. **Girod, A., C. E. Wobus, Z. Zadori, M. Ried, K. Leike, P. Tijssen, J. A. Kleinschmidt, and M. Hallek.** 2002. The VP1 capsid protein of adeno-associated virus type 2 is carrying a phospholipase A2 domain required for virus infectivity. J. Gen. Virol. **83:**973–978.
13. **Glotzer, J. B., A. I. Michou, A. Baker, M. Saltik, and M. Cotten.** 2001. Microtubule-independent motility and nuclear targeting of adenoviruses with fluorescently labeled genomes. J. Virol. **75:**2421–2434.
14. **Grimm, D., A. Kern, M. Pawlita, F. Ferrari, R. Samulski, and J. Kleinschmidt.** 1999. Titration of AAV-2 particles via a novel capsid ELISA: packaging of genomes can limit production of recombinant AAV-2. Gene Ther. **6:**1322–1330.
15. **Hacker, U. T., F. M. Gerner, H. Buning, M. Hutter, H. Reichenspurner, M. Stangl, and M. Hallek.** 2001. Standard heparin, low molecular weight heparin, low molecular weight heparinoid, and recombinant hirudin differ in their ability to inhibit transduction by recombinant adeno-associated virus type 2 vectors. Gene Ther. **8:**966–968.
16. **Hansen, J., K. Qing, and A. Srivastava.** 2001. Adeno-associated virus type 2-mediated gene transfer: altered endocytic processing enhances transduction efficiency in murine fibroblasts. J. Virol. **75:**4080–4090.
17. **High, K. A.** 2004. Clinical gene transfer studies for hemophilia B. Semin. Thromb. Hemost. **30:**257–267.
18. **Hoque, M., K. Ishizu, A. Matsumoto, S. I. Han, F. Arisaka, M. Takayama, K. Suzuki, K. Kato, T. Kanda, H. Watanabe, and H. Handa.** 1999. Nuclear transport of the major capsid protein is essential for adeno-associated virus capsid formation. J. Virol. **73:**7912–7915.
19. **Kronenberg, S., B. Bottcher, C. W. von der Lieth, S. Bleker, and J. A. Kleinschmidt.** 2005. A conformational change in the adeno-associated virus type 2 capsid leads to the exposure of hidden VP1 N termini. J. Virol. **79:**5296–5303.
20. **Loiler, S. A., T. J. Conlon, S. Song, Q. Tang, K. H. Warrington, A. Agarwal, M. Kapturczak, C. Li, C. Ricordi, M. A. Atkinson, N. Muzyczka, and T. R. Flotte.** 2003. Targeting recombinant adeno-associated virus vectors to enhance gene transfer to pancreatic islets and liver. Gene Ther. **10:**1551–1558.
21. **McDonald, D., M. A. Vodicka, G. Lucero, T. M. Svitkina, G. G. Borisy, M. Emerman, and T. J. Hope.** 2002. Visualization of the intracellular behavior of HIV in living cells. J. Cell Biol. **159:**441–452.
22. **Mizukami, H., N. S. Young, and K. E. Brown.** 1996. Adeno-associated virus

type 2 binds to a 150-kilodalton cell membrane glycoprotein. Virology **217:** 124–130.
23. **Mouw, M. B., and D. J. Pintel.** 2000. Adeno-associated virus RNAs appear in a temporal order and their splicing is stimulated during coinfection with adenovirus. J. Virol. **74:**9878–9888.
24. **Ried, M. U., A. Girod, K. Leike, H. Buning, and M. Hallek.** 2002. Adeno-associated virus capsids displaying immunoglobulin-binding domains permit antibody-mediated vector retargeting to specific cell surface receptors. J. Virol. **76:**4559–4566.
25. **Sampaio, K. L., Y. Cavignac, Y. D. Stierhof, and C. Sinzger.** 2005. Human cytomegalovirus labeled with green fluorescent protein for live analysis of intracellular particle movements. J. Virol. **79:**2754–2767.
26. **Samulski, R. J., K. I. Berns, M. Tan, and N. Muzyczka.** 1982. Cloning of adeno-associated virus into pBR322: rescue of intact virus from the recombinant plasmid in human cells. Proc. Natl. Acad. Sci. USA **79:**2077–2081.
27. **Seisenberger, G., M. U. Ried, T. Endress, H. Buning, M. Hallek, and C. Brauchle.** 2001. Real-time single-molecule imaging of the infection pathway of an adeno-associated virus. Science **294:**1929–1932.
28. **Shi, W., G. S. Arnold, and J. S. Bartlett.** 2001. Insertional mutagenesis of the adeno-associated virus type 2 (AAV2) capsid gene and generation of AAV2 vectors targeted to alternative cell-surface receptors. Hum. Gene Ther. **12:** 1697–1711.
29. **Suomalainen, M., M. Y. Nakano, S. Keller, K. Boucke, R. P. Stidwill, and U. F. Greber.** 1999. Microtubule-dependent plus- and minus end-directed motilities are competing processes for nuclear targeting of adenovirus. J. Cell Biol. **144:**657–672.
30. **Theiss, H. D., D. M. Kofler, H. Buning, A. L. Aldenhoff, B. Kaess, T. Decker, J. Baumert, M. Hallek, and C. M. Wendtner.** 2003. Enhancement of gene transfer with recombinant adeno-associated virus (rAAV) vectors into primary B-cell chronic lymphocytic leukemia cells by CpG-oligodeoxynucleotides. Exp. Hematol. **31:**1223–1229.
31. **Wagner, J. A., I. B. Nepomuceno, A. H. Messner, M. L. Moran, E. P. Batson, S. Dimiceli, B. W. Brown, J. K. Desch, A. M. Norbash, C. K. Conrad, W. B. Guggino, T. R. Flotte, J. J. Wine, B. J. Carter, T. C. Reynolds, R. B. Moss, and P. Gardner.** 2002. A phase II, double-blind, randomized, placebo-controlled clinical trial of tgAAVCF using maxillary sinus delivery in patients with cystic fibrosis with antrostomies. Hum. Gene Ther. **13:**1349–1359.
32. **Ward, B. M.** 2004. Pox, dyes, and videotape: making movies of GFP-labeled vaccinia virus. Methods Mol. Biol. **269:**205–218.
33. **Warrington, K. H., Jr., O. S. Gorbatyuk, J. K. Harrison, S. R. Opie, S. Zolotukhin, and N. Muzyczka.** 2004. Adeno-associated virus type 2 VP2 capsid protein is nonessential and can tolerate large peptide insertions at its N terminus. J. Virol. **78:**6595–6609.
34. **Wistuba, A., A. Kern, S. Weger, D. Grimm, and J. A. Kleinschmidt.** 1997. Subcellular compartmentalization of adeno-associated virus type 2 assembly. J. Virol. **71:**1341–1352.
35. **Wobus, C. E., B. Hugle-Dorr, A. Girod, G. Petersen, M. Hallek, and J. A. Kleinschmidt.** 2000. Monoclonal antibodies against the adeno-associated virus type 2 (AAV-2) capsid: epitope mapping and identification of capsid domains involved in AAV-2-cell interaction and neutralization of AAV-2 infection. J. Virol. **74:**9281–9293.
36. **Wu, P., W. Xiao, T. Conlon, J. Hughes, M. Agbandje-McKenna, T. Ferkol, T. Flotte, and N. Muzyczka.** 2000. Mutational analysis of the adeno-associated virus type 2 (AAV2) capsid gene and construction of AAV2 vectors with altered tropism. J. Virol. **74:**8635–8647.
37. **Xiao, W., K. H. Warrington, Jr., P. Hearing, J. Hughes, and N. Muzyczka.** 2002. Adenovirus-facilitated nuclear translocation of adeno-associated virus type 2. J. Virol. **76:**11505–11517.
38. **Xiao, X., J. Li, and R. J. Samulski.** 1998. Production of high-titer recombinant adeno-associated virus vectors in the absence of helper adenovirus. J. Virol. **72:**2224–2232.
39. **Yang, Q., M. Mamounas, G. Yu, S. Kennedy, B. Leaker, J. Merson, F. Wong-Staal, M. Yu, and J. R. Barber.** 1998. Development of novel cell surface CD34-targeted recombinant adenoassociated virus vectors for gene therapy. Hum. Gene Ther. **9:**1929–1937.
40. **Zadori, Z., J. Szelei, M. C. Lacoste, Y. Li, S. Gariepy, P. Raymond, M. Allaire, I. R. Nabi, and P. Tijssen.** 2001. A viral phospholipase A2 is required for parvovirus infectivity. Dev. Cell **1:**291–302.
41. **Zolotukhin, S., B. J. Byrne, E. Mason, I. Zolotukhin, M. Potter, K. Chesnut, C. Summerford, R. J. Samulski, and N. Muzyczka.** 1999. Recombinant adeno-associated virus purification using novel methods improves infectious titer and yield. Gene Ther. **6:**973–985.